Bulletin of Geophysics and Oceanography
Vol. XX, n. X, pp. XXX-XXX; Xxxxx 20xx
DOI 10.4430/bgo00485

Stress accumulation on the Karlıova (Bingöl) Triple Junction after two big earthquakes (Pazarcık-Ekinözü) in Turkey in 2023

Ö. Bektaş[1], A. Pirti[2], H. Alkan[3], M.A. Yücel[4] and A. Büyüksaraç[5]

[1] *Department of Geophysical Engineering, Sivas Cumhuriyet University, Sivas, Turkey*
[2] *Department of Geomatics Engineering, Yildiz Technical University, Istanbul, Turkey*
[3] *Department of Geophysical Engineering, Van Yüzüncü Yıl University, Van, Turkey*
[4] *Department of Geomatics Engineering, Canakkale Onsekiz Mart University, Çanakkale, Turkey*
[5] *Çanakkale Onsekiz Mart University, Çan Vocational School, Çanakkale, Turkey*

(Received: 13 May 2024; accepted: 21 November 2024; published online: 23 May 2025)

ABSTRACT Active fault zones primarily influence earthquakes in the Karlıova (Bingöl) region. The mentioned region is in Turkey's first and second seismic hazard zones; however, it also includes certain areas in the third and fourth seismic hazard zones. In this study, we investigated the earthquake activities using data collected from various global navigation satellite system (GNSS) surveys of continuously operating reference stations in Turkey (CORS-TR). We also analysed the Coulomb stress change caused by the 15 local earthquakes surrounding the Karlıova Triple Junction. Additionally, we investigated the relationship between Coulomb stress change and horizontal displacements from GNSS survey results, focusing on horizontal displacement vectors. Besides, gravity data were used to infer the fault geometries and shallow crustal structures. The largest horizontal movement was observed at the BIN1 station, the intersection point of the North Anatolian Fault Zone (NAFZ) and the East Anatolian Fault Zone (EAFZ). At the CORS-TR point on the Karlıova segment of the EAFZ, the horizontal displacement was calculated to be approximately 10.1 cm in the north-eastern direction. The observations of Coulomb stress change reveal that positive stress variations were observed in the NW-SE and SW-NE directions along the main fault line at a depth of approximately 30 km, in accordance with the tilt transformation of gravity anomalies.

Key words: earthquake, GNSS, horizontal displacement, Coulomb stress change, gravity, Karlıova Triple Junction.

1. Introduction

The Karlıova Triple Junction (KTJ) is located in the eastern part of Turkey and is a continental collision zone associated with the Arabian, Eurasian, and Anatolian plates. In this region, there are two major tectonic structures: the North Anatolian Fault Zone (NAFZ) and the Eastern Anatolian Fault Zone (EAFZ). These fault systems meet at the KTJ, to the north of the Bitlis-Zagros Suture Zone (BZSZ). The KTJ is the pivot point of transtensional deformation and is considered the easternmost boundary of the westward motion of the Anatolian Plate relative to the Eurasian Plate (McKenzie, 1972; Şengör, 1979; Aktug *et al.*, 2013; Karaoğlu *et al.*, 2016; Di Giuseppe *et al.*, 2017). With a complicated structural setting, the Varto Fault Zone (VFZ), located near the eastern part of the KTJ, also stands out as the adjacent secondary important structure in the region. The VFZ, starting at the south of the KTJ and continuing eastwards, is composed of three segments namely the Varto, Leylekdağ, and Çayçatı segments (Sançar *et al.*, 2015). The right lateral strike-slip fault system characterises the VFZ and has a length of approximately 30 km along a widely distributed zone (Sançar *et al.*, 2015; Emre *et al.*, 2018). This region is characterised by the occurrence of high-energy earthquakes.

The EAFZ is a left-lateral strike-slip fault spanning about 580 km, with an average slip rate of approximately 10 mm per year (Fig. 1). It marks the active boundary between the Anatolian and Arabian plates, running NE-SW from Karlıova, Bingöl, where it joins the NAFZ, to the Kahramanmaraş Triple Junction at the northern terminus of the Dead Sea Fault Zone (DSFZ) (Şengör, 1979; Reilinger and McClusky, 2011; Duman and Emre, 2013; Emre *et al.*, 2018; Alkan *et al.*, 2024). Earth scientists have investigated whether the EAFZ, which is divided into six main fault segments (the Karlıova-Bingöl, Palu-Hazar, Hazar Lake-Sincik, Çelikhan-Erkenek, Gölbaşı-Türkoğlu, and Türkoğlu-Antakya segments), has ruptured or released its energy (Akar *et al.*, 2024). The evidence is that the 2023 Kahramanmaraş earthquakes (M_w = 7.7 and M_w = 7.6) occurred in the Amanos-Pazarcık-Erkenek and Savrun-Çardak segments, respectively (Barbot *et al.*, 2023).

Conversely, the NAFZ is one of the most known strike-slip mechanisms in the Alpine-Himalayan orogenic belt and has produced, in both historical and instrumental times, devastating earthquakes (M_w = 7.0+), such as the Gölcük (İzmit) (M_w = 7.6) and Kaynaşlı (Düzce) (M_w = 7.2) earthquakes in 1999. The NAFZ consists of 38 segments, with significant segments including the Yedisu, Erzincan, Ezinepazar, Dokurcun, and Ganos segments (Şengör *et al.*, 2005; Reilinger *et al.*, 2006; Emre *et al.*, 2018; Işık *et al.*, 2021; Işık, 2022; Poyraz, 2023; Caroir *et al.*, 2024; Seyitoğlu *et al.*, 2024).

There are important basin areas in and around the KTJ that are associated with the current tectonic and seismic activity of the region. One of these important basins is the Bingöl Basin (BB), located in the eastern part of the upper Euphrates section of the eastern Anatolia region of Turkey. The BB is one of the pull-apart tectonic basins formed on the EAFZ and is one of the important active structural elements of Turkey (Sarp, 2014; Akbayram *et al.*, 2022). The BB comprises Paleozoic-Lower Mesozoic metamorphics, Upper Cretaceous ophiolitic mélange, Eocene-Lower Miocene marine sedimentary, and volcano-sedimentary deposits. During the neotectonic period, due to the continent-continent collision, the BB was affected by the segments of the EAFZ and the Karakoçan-Bingöl Fault Zone (Şengör, 1980; Kıranşan *et al.*, 2021). Another important basin is the Erzincan Basin (EB), one of the few Neogene sedimentary basins developed by long-term right-lateral strike-slip along the NAFZ. The BB is an intracontinental transform fault that defines the current boundary between the Eurasian Plate, to the north, and the Anatolian Plate, to the south. The basin has a young volcanic centre with an asymmetric and widespread development of cross faults that define an advanced stage of pull-apart basin evolution. A model has been developed for the EB evolution, which probably started with a simple separation with a right-lateral strike-slip on the NAFZ and developed in the early Pliocene period. Later, interaction with a large left-lateral Ovacık Fault (OF) (Fig. 1) caused the focus of movement in the NAFZ to shift to the SW resulting in the development of a complex herringbone fracture system. It has become the focus of volcanic activity on three lineaments that extend southwards towards the basin axis. Continuous movement on the OF has transformed the south-eastern margin of the basin into an extensional zone, and the tectonic history of the basin is further complicated by its proximity to a major transform intersection between the NAFZ and OF (Akpinar *et al.*, 2016). The third important basin is the Karlıova Basin located at the easternmost point of the Anatolian Plate, which holds a significant place in the neotectonics of Anatolia. The basin corresponds to the KTJ region, where the NAFZ, EAFZ, and VFZ intersect. The basin developed as a fault-wedge basin due to the NAFZ and EAFZ movement in different directions and opens to external drainage due to the backward erosion of the Göynük Stream in the Quaternary.

This paper aims to evaluate the general geomorphology, stress transfer, and gravity anomaly distribution of the KTJ and its surroundings and to explain the morphometric indices determined

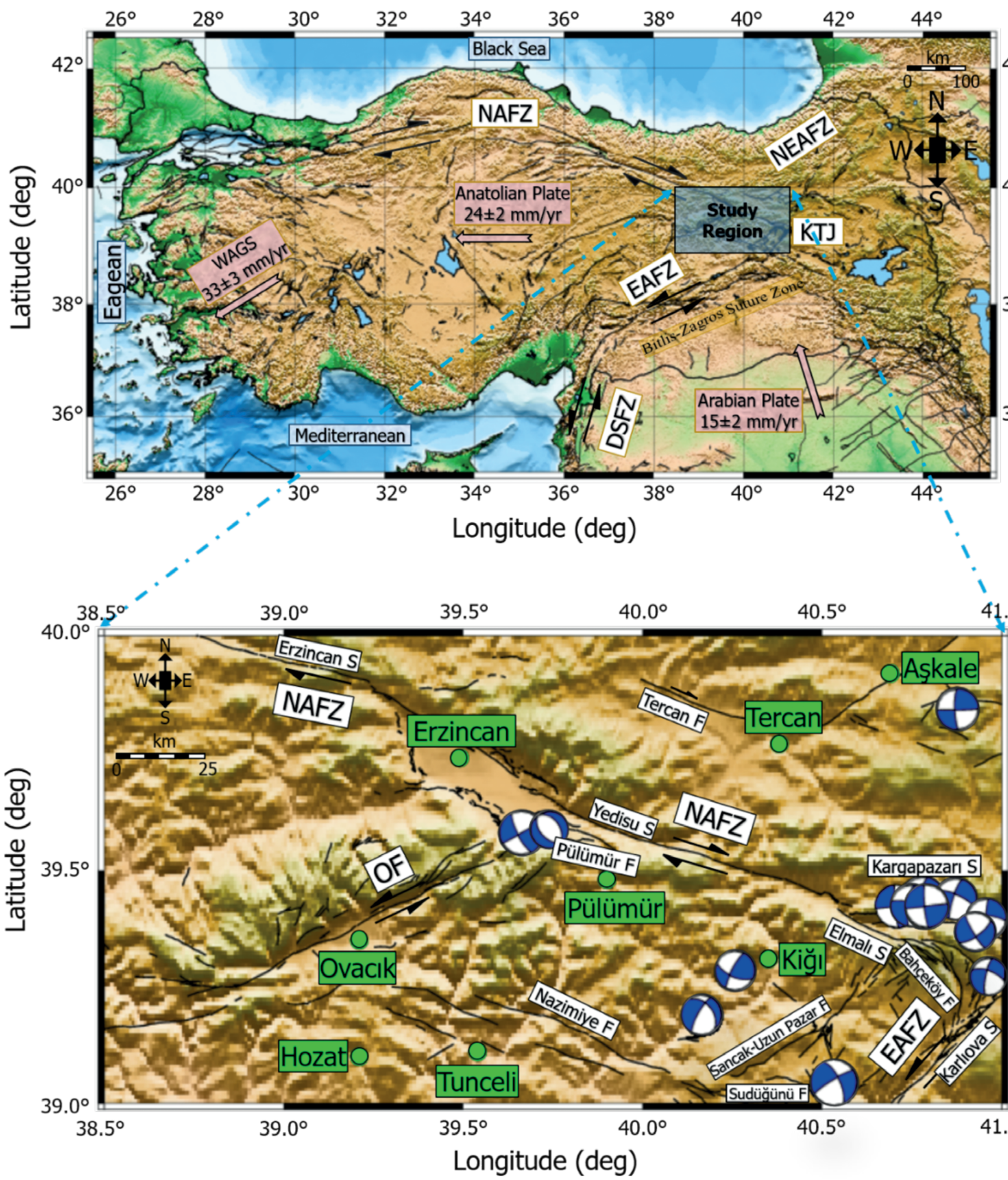

Fig. 1 - Top) Location of the study region with the main tectonic elements in and around the Anatolian region (modified from Emre *et al.*, 2018; Alkan *et al.*, 2023; Büyüksaraç *et al.*, 2024). The blue rectangle represents the study region. The pink arrows show the direction of plate motions with velocities (modified from Reilinger *et al.*, 2006). Bottom) Focal mechanism solution distributions of the earthquakes with $M_L \geq 5.0$ between 2003 and 2021 that occurred in the study region. The black arrows represent the direction of movement of fault and fault zones (taken from Emre *et al.*, 2018). The green circles represent the province locations. Abbreviations: NAFZ = North Anatolian Fault Zone, NEAFZ = NE Anatolian Fault Zone, EAFZ = East Anatolian Fault Zone, DSFZ = Dead Sea Fault Zone, KTJ = Karlıova Triple Junction, WAGS = West Anatolian Graben System, OF = Ovacık Fault, S = segment, F = fault.

in the fault zones through lineament analysis. The Coulomb stress change maps are created with vertical cross-sections to identify the high- or low-stress regions. Then, the horizontal and vertical displacement vectors are investigated using the GNSS techniques and local earthquake vectors.

The Kahramanmaraş earthquakes experienced in 2023 showed that stress transfer can occur quite effectively. Stress accumulation, especially over long periods, can cause very rapid stress transfer. As the EAFZ had such a feature, stress transfer caused it to move very quickly first southwards, then westwards, and, finally, northwards. From this aspect, our comprehensive analysis was carried out on the stress accumulation and structural properties in the KTJ and surroundings after the Kahramanmaraş (Turkey) earthquakes in 2023.

2. Seismicity of the study region

The Anatolia region presents very intensive seismicity in the shallow crust due to the rapid movement of tectonic elements, with many destructive earthquakes occurring in the historical and instrumental periods. For example, the Gölcük (Kocaeli) earthquake (M_w = 7.6) of 17 August 1999 and the Kaynaşlı (Düzce) earthquake (M_w = 7.2) of 12 November 1999 occurred in the NAFZ at the eastern end of the Marmara Sea (Ambraseys and Jackson, 2000). The Bingöl earthquake (M_w = 6.4) occurred on 1 May 2003. This event was approximately 60 km SW of the KTJ (Öztürk *et al.*, 2008). After the mainshock, approximately 516 aftershocks were recorded by seismic stations. The Bingöl aftershock sequences showed that the north and west of the Bingöl province reflected the high-stress regions associated with lower *b*-values. The Van earthquake (M_w = 7.2) of 23 October 2011 hit the Van region and caused significant damage in Van city, resulting in a total life loss of 644 (Erdik *et al.*, 2012). In addition, the Sivrice (Elazığ) earthquake (M_w = 6.8) of 24 January 2020 created positive stress transfer along the segments of the EAFZ (around Palu-Hazar Lake and Çelikhan-Gölbaşı) in the NE and SW directions (Alkan *et al.*, 2021). According to Alkan *et al.* (2021), these segments reflected potential zones of future great earthquakes. The aftershocks, characteristic of the Sivrice (Elazığ) earthquake, were investigated by Öztürk (2023) who calculated the lowest *b*-values derived from the Gutenberg-Richter formula and the largest *p*-values from the modified Omori law in the north, south, and SW parts of the mainshock including the Pütürge and Erkenek segments. In 2023, two devastating earthquakes with moment magnitudes M_w = 7.7 and M_w = 7.6 occurred on 6 February 2023, in the Pazarcık and Elbistan provinces, causing great destruction to the surrounding cities of Kahramanmaraş, Adana, Hatay, Osmaniye, Kilis, Gaziantep, Adıyaman, Malatya, Şanlıurfa, Diyarbakır, and Elazığ (AFAD, 2024). The earthquake catalogue indicates that more than 62,000 aftershocks have been recorded on the seismic stations in the region to this day. These devastating earthquakes, with their aftershocks, caused more than 50,000 people to lose their lives and destroyed around 550,000 houses (Işık *et al.*, 2023).

The KTJ and its surroundings have been affected by destructive earthquakes in historical and instrumental periods. There are many primary and secondary faults and fault zones such as the NAFZ, EAFZ, OF, Tercan Fault, and Nazimiye Fault in the region (Fig. 1). According to historical records of the AFAD (the Turkish Disaster and Emergency Management Presidency) catalogue, the events with intensity greater than IX occurred in and around the Erzincan province in the 1000s and 1800s. Also, Fig. 1 shows the focal mechanism solutions and epicentre locations of the events with a magnitude greater than M_L > 5.0 from 2003 to 2021, generally indicating strike-slip fault mechanisms. In addition, earthquakes with magnitude M_w ≥ 3.0 recorded since the beginning of the instrumental recordings and depicted in Fig. 2, consist of approximately 2,700 earthquakes that occurred in the region. These instrumental earthquakes are clustered close to active faults and fault zones. The most important of these earthquakes was the 27 December 1939 Erzincan earthquake (M_S = 7.9) that occurred on the NAFZ. The 1939 Erzincan earthquake is Turkey's largest recorded earthquake with a 360-km long surface rupture, killing around 33,000 people (Aktug *et al.*, 2013; Gürsoy *et al.*, 2013; Işık, 2022). Moreover, it is very important to investigate the activity level of the Yedisu Seismic Gap (YSG) located between Bingöl and Karlıova with a length of approximately 70 km, which is considered one of the most important seismic gaps. The YSG comprises some sub-segments of the NAFZ called Kargapazarı, Elmalı, Yedisu, and Erzincan (Emre *et al.*, 2018; Alkan *et al.*, 2023). The fact that this seismic gap has not produced a significant earthquake (M ≥ 7.0) since 1784 is very important in terms of earthquake hazard potential (Sançar and Akyüz, 2014; Zabcı *et al.*, 2017). Seismologists predict that a devastating earthquake will soon occur in the YSG.

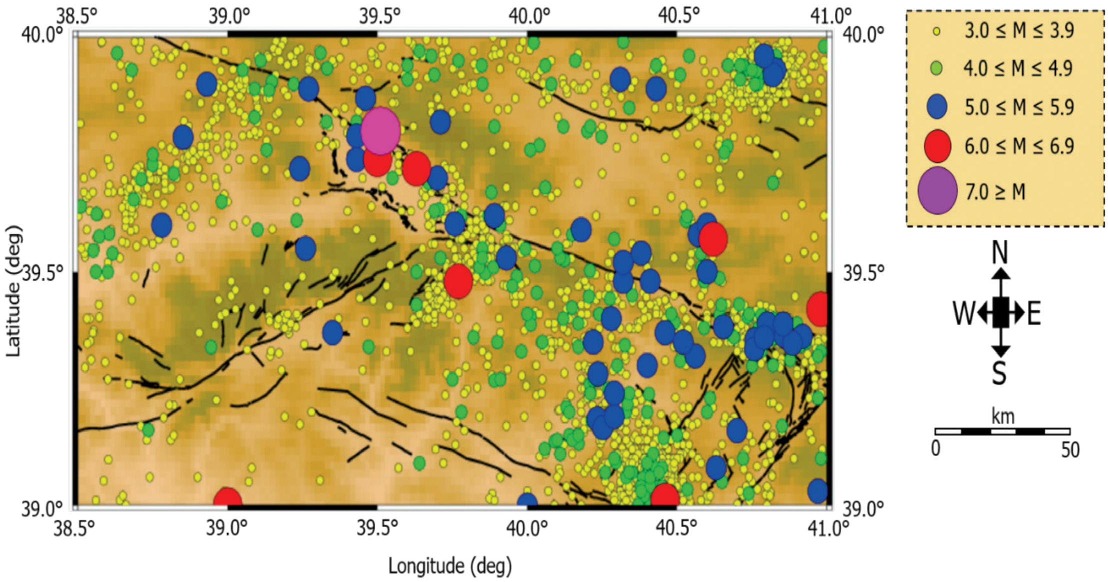

Fig. 2 - Epicentre locations of 2662 earthquakes with M_w ≥ 3.0 from 1 Jan 1900 to 1 Mar 2024 for the study region. The seismicity catalogue is obtained from the KOERI (2024) website. Magnitude levels of the events are shown with circles of different colors and sizes.

3. Methods

3.1. Gravity anomalies

The data used in this study were provided by the General Directorate of Mineral Research and Exploration (Turkey) (MTA) in the form of a 10-kilometre grid. MTA has carried out 62,000 gravity measurements at 2-5 km station intervals during many years of work in Turkey and published the Bouguer gravity anomaly map (Ateş *et al.*, 1999) using a density of 2.67 g/cm^3. MTA applied all corrections made to the measured gravity values. Gravity anomalies in Turkey generally show E-W oriented contours, and most of the land area is characterised by negative anomalies reflecting the isostatically thickened continental crust, which increases in thickness towards the east. The gravity anomaly map of the study region is shown in Fig. 3.

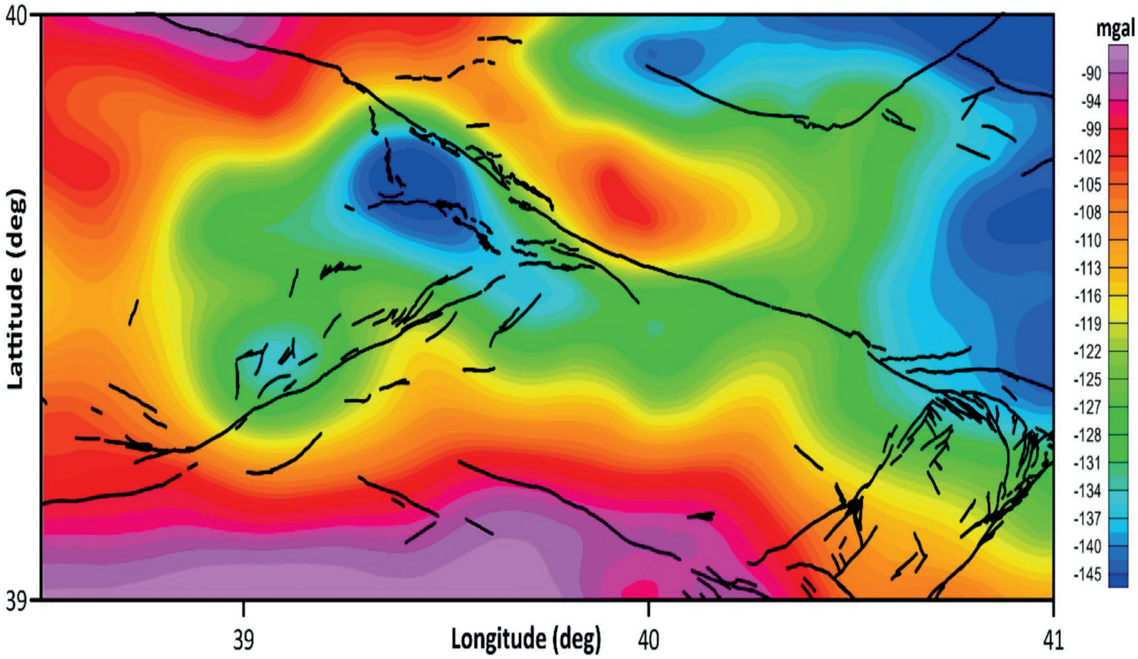

Fig. 3 - Gravity anomaly map of the study region. The gravity data with 10-kilometre gridded and active fault lines were obtained from MTA.

The use of a total horizontal derivative (*THD*) filter, which is the first generation of edge detection filters, is now standard. The *THD* filter is given by Cordell and Grauch (1985) as:

$$THD = \sqrt{\left(\frac{\partial M}{\partial x}\right)^2 + \left(\frac{\partial M}{\partial y}\right)^2} \tag{1}$$

where *M* is the gravity data. The highest amplitude values of the anomalies were obtained as a result of the *THD* passing over the geological and tectonic structure boundaries. Even with the second derivative in the *THD* method, the zero value does not precisely coincide with the edge of the structure and the resolution varies across all these measures when multiple sources are present. This situation is considered a weakness of the method. To overcome this, the first developed filter is the Tilt Angle (*TA*) filter given by Miller and Singh (1994), as:

$$TA = \tan^{-1}\left(\frac{\frac{\partial M}{\partial z}}{THD}\right). \tag{2}$$

The *TA* is obtained by normalising the vertical derivative relative to the *THD*. The *THD* and *TA* filters were applied to gravity data shown in Fig. 3 to determine the boundaries and lineaments of the structures in the study area. The *THD* map (shown in Fig. 4) was found to be compatible with the existing geological formations and discontinuities in the study area. The *TA* map is shown in Fig. 5. The *TA* reflects the effects of both near-surface and deep sources at the same amplitude level. The amplitude of the *TA* is positive when on the structure, zero when on the edge of the structure, and negative outside the structure. The amplitude values range between –π/2 and π/2, making it very easy to interpret. The results of the *TA* derivative method were compared with the existing discontinuities and geological elements in the study area. The amplitude of the *TA* is +1.5 (π/2) (pink) when it is on the structure, 0 (yellow) when it is on the edge of the structure, and the discontinuities (continuous black lines) are compatible with the *TA* values.

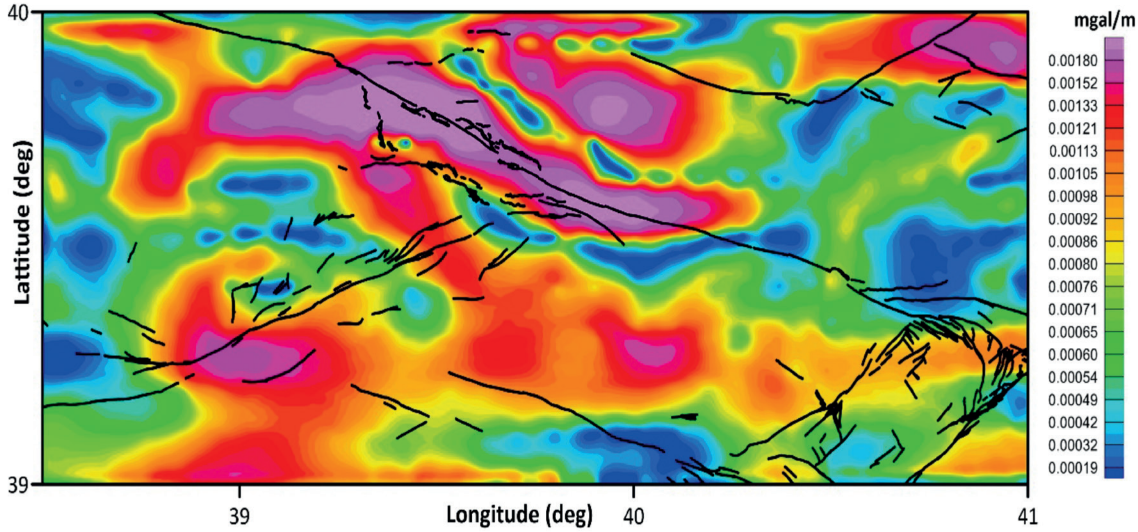

Fig. 4 - *THD* map of the study area.

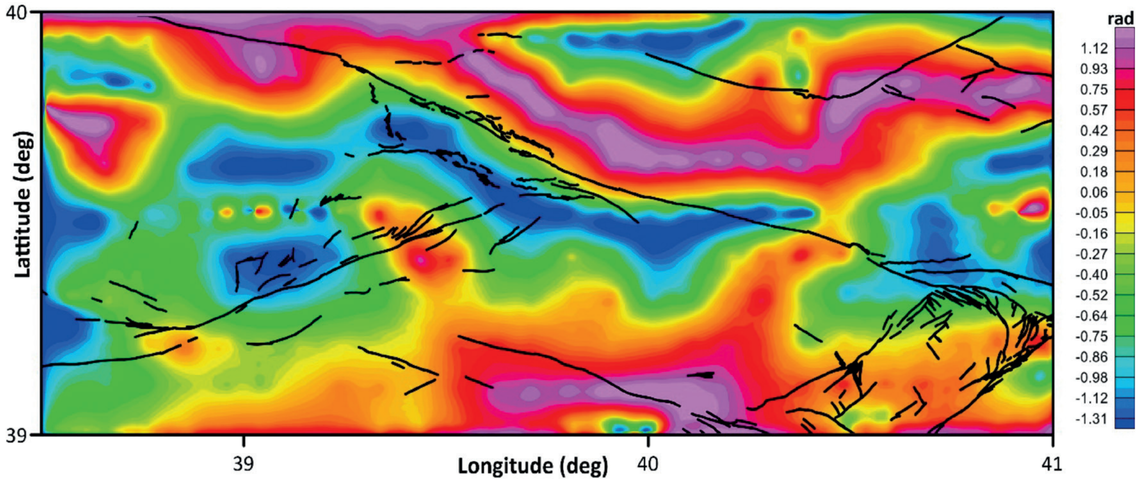

Fig. 5 - *TA* map of the study region.

3.2. GNSS surveys

GNSS surveys are frequently used in studies on geodynamics and geodetic modelling, cartography studies, and crustal movements. This method is used to determine ground deformations caused by earthquakes. Additionally, GNSS is a valuable data source for defining geological and atmospheric phases (Pırtı, 2022; Gunaydin *et al.*, 2023; Pırtı *et al.*, 2023; Yücel *et al.*, 2024). The millimetre-scale movements of the crust between earthquakes are measured by GNSS observations (Pırtı, 2024). In this context, data from ten GNSS stations of the CORS-TR network close to the earthquake epicentre are particularly helpful. However, the data from these reference stations, recorded at intervals of 1 to 30 s, are particularly useful in identifying crustal deformations and earthquakes. Understanding the degree of stress caused by the two earthquakes is necessary for comprehending the tectonic processes involved in the Bingöl-Erzincan-Tunceli triple region. The stations of the CORS-TR network near the earthquake epicentre provided very useful data.

Data were gathered and processed for 10 stations of the CORS-TR network near the epicentre of the Kahramanmaraş earthquakes (Figs. 6 and 7; Tables 1 to 4). These 10 CORS-TR points were located approximately 10-500 km away from the earthquake centres (Pazarcık and Ekinözü in Kahramanmaraş), as shown in Figs. 6 and 7. 24-hour receiver independent exchange format (RINEX) observation data with 30-second intervals were downloaded from the CORS-TR servers.

In this study, Topcon Magnet Tools v.8.2.0 software (Topcon, 2024) was used to process the GNSS data. Topcon Magnet Tools is a comprehensive suite for managing and processing GNSS data. It enables users to handle raw GNSS data, perform baseline processing, and analyse the results with high precision. The software enables post-processing and adjusting of field survey data collected by GNSS equipment. The software supports static and kinematic GNSS positioning, making it suitable for various geodetic applications. In this context, the 24-hour RINEX observation files with 30-second intervals, obtained from the stations of the CORS-TR network, were processed using the static technique within the software. Using Topcon Magnet Tools, the 24-hour RINEX

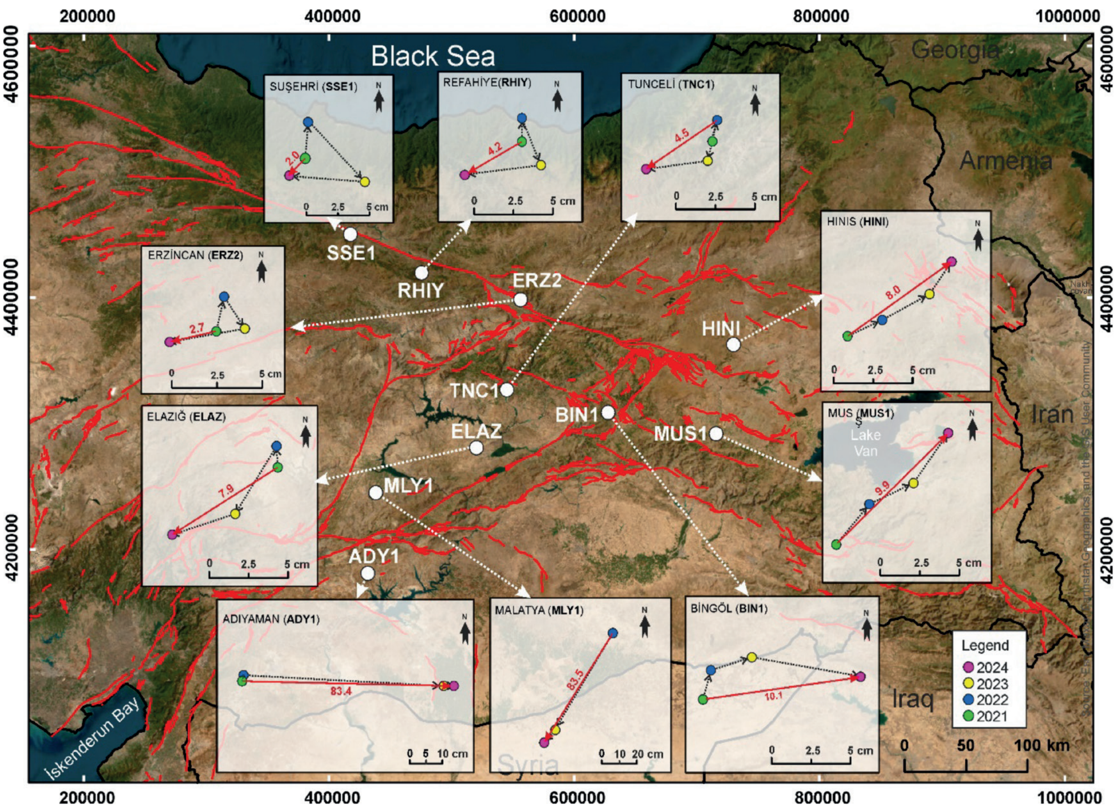

Fig. 6 - Map of the observed GNSS stations and horizontal velocities between 2021 and 2024.

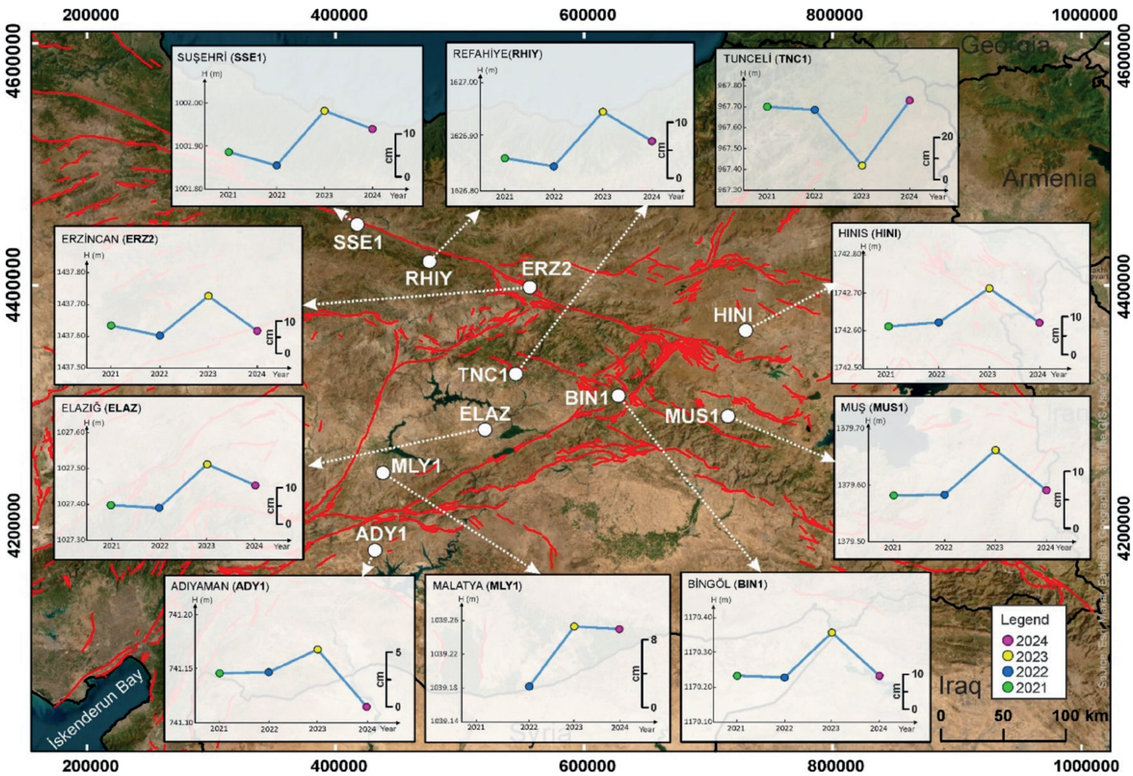

Fig. 7 - Map of the observed GNSS stations and vertical velocities between 2021 and 2024.

observation files (6 February 2021, 2022, 2023, and 2024) from the 10 stations of the CORS-TR network were analysed with a 30-second interval between 00:00:00-02:00:00 UTC.

Static processing results were obtained from Topcon Magnet Tools v.8.2.0 (24 hours). During the monitoring period (23 November 2022), the standard deviations of the coordinates were calculated with an accuracy of 2 mm in the horizontal components and 8-9 mm in the vertical

Table 1 - GNSS locations and standard deviations on 6 February 2021 (no GNSS data were recorded at station MLY1 on this date).

No.	Grid northing (m)	Grid easting (m)	Elevation (m)	North std dev (cm)	East std dev (cm)	Up std dev (cm)
ADY1	4181181.128	434902.239	741.146	1.2	1.1	2.8
BIN1	4308167.635	630368.564	1170.234	1.0	0. 9	2.2
ELAZ	4279089.861	522327.511	1027.399	1.0	0.9	2.4
ERZ2	4397324.612	559776.307	1437.634	1.0	0.9	2.4
HINI	4362914.982	732326.561	1742.613	1.0	0.9	2.3
MUS1	4293000.897	717290.344	1379.582	0.0	0.0	0.0
RHIY	4419129.753	480401.054	1626.86	1.0	1.0	2.4
SSE1	4448690.584	423762.389	1001.886	1.1	1.0	2.6
TNC1	4327004.706	546287.147	967.702	1.0	0.9	2.3

Table 2 - GNSS locations and standard deviations on 6 February 2022.

No.	Grid northing (m)	Grid easting (m)	Elevation (m)	Elevation change (cm)	North std dev (cm)	East std dev (cm)	Up std dev (cm)
ADY1	4181181.145	434902.244	741.147	+0.1	0.9	1.2	2.4
BIN1	4308167.653	630368.569	1,170.229	-0.5	0.9	0.8	2.2
ELAZ	4279089.874	522327.510	1,027.391	-0.8	0.9	0.9	2.2
ERZ2	4397324.625	559776.310	1,437.602	-3.2	0.9	0.9	2.3
HINI	4362914.992	732326.583	1,742.624	+1.1	0.9	0.9	2.2
MLY1	4245676.781	440426.237	1,039.182	No data	0.9	0.1	2.4
MUS1	4293000.922	717290.365	1,379.583	+0.1	0.0	0.0	0.0
RHIY	4419129.765	480401.054	1,626.845	-1.5	0.9	0.1	2.3
SSE1	4448690.597	423762.390	1,001.855	-3.1	0.1	1.1	2.5
TNC1	4327004.719	546287.150	967.687	-1.5	0.9	0.9	2.2

Table 3 - GNSS locations and standard deviations on 6 February 2023.

No.	Grid northing (m)	Grid easting (m)	Elevation (m)	Elevation change (cm)	North std dev (cm)	East std dev (cm)	Up std dev (cm)
ADY1	4181181.110	434903.033	741.168	+2.1	1.0	1.1	2.5
BIN1	4308167.661	630368.595	1170.358	+12.9	0.9	0.9	2.2
ELAZ	4279089.832	522327.484	1027.513	+12.2	0.9	0.1	2.2
ERZ2	4397324.613	559776.318	1437.727	+12.5	0.9	0.1	2.2
HINI	4362915.008	732326.613	1742.715	+9.1	0.9	0.9	2.2
MLY1	4245676.152	440425.865	1039.253	+7.1	0.9	0.1	2.4
MUS1	4293000.935	717290.393	1379.662	+7.9	0.0	0.0	0.0
RHIY	4419129.741	480401.064	1626.945	+10.0	0.9	0.1	2.3
SSE1	4448690.576	423762.410	1001.981	+12.6	0.1	1.1	2.4
TNC1	4327004.694	546287.144	967.420	-26.7	0.9	0.9	2.2

Table 4 - GNSS locations and standard deviations on 6 February 2024.

No.	Grid northing (m)	Grid easting (m)	Elevation (m)	Elevation change (cm)	North std dev (cm)	East std dev (cm)	Up std dev (cm)
ADY1	4181181.109	434903.073	741.115	-5.3	1.1	1.0	2.6
BIN1	4308167.649	630368.664	1170.234	-12.4	1.1	0.9	2.3
ELAZ	4279089.819	522327.444	1027.454	-5.9	0.9	0.8	2.3
ERZ2	4397324.608	559776.289	1437.617	-11.0	1.0	0.9	2.3
HINI	4362915.028	732326.627	1742.623	-9.2	0.9	0.8	2.3
MLY1	4245676.080	440425.783	1039.250	-0.3	1.0	0.9	2.4
MUS1	4293000.966	717290.415	1379.591	-7.1	0.0	0.0	0.0
RHIY	4419129.736	480401.024	1626.891	-5.4	1.0	0.9	2.4
SSE1	4448690.578	423762.383	1001.939	-4.2	1.1	1.0	2.6
TNC1	4327004.689	546287.105	967.732	+31.2	1.0	0.8	2.3

components. The impact of the earthquake was lowest on the ERZ2 station. Static processing was performed by considering the ERZ2 station as fixed (ITRF 20 Epoch, 2024) (Fig. 7).

The horizontal movements are calculated, respectively, as 83.5 cm at the MLY1, 7.9 cm at the ELAZ, 4.5 cm at the TNC1, 2.7 cm at the ERZ2, 4.2 cm at the RHIY, and 2.0 at the SSE1 stations, all in the SW direction. In the same period, the horizontal movements are calculated, respectively, as 10.1 cm at the BIN1 and 8.0 cm at the HINI stations, both in the NE direction.

The elevation values of the CORS-TR GNSS stations, computed between 2021 and 2024 (Tables 1 to 4), along with the annual height changes, are shown in Fig. 7. The ADY1 point swelled by 2.1 cm during the earthquake and sank by 5.3 cm in the first year after the earthquake; the BIN1 point swelled by 12.9 cm after the earthquake and sank by 12.4 cm; the ELAZ point swelled by 12.2 cm at the time of the earthquake and sank by 5.9 cm in the following year; and the ERZ2 point swelled by 12.5 cm and sank by 11 cm; the HINI point swelled by 9.1 cm and sank by 9.2 cm in the next year; the MLY1 point swelled by 7.1 cm and sank by 0.3 cm; the MUS1 point swelled by 7.9 cm and sank by 7.7 cm; and the RHIY point swelled by 10 cm with the earthquake and sank by 5.4 cm. It was calculated that the SSE1 point swelled by 12.6 cm and, then, collapsed by 4.2 cm. Ultimately, the TNC1 point swelled by 3 cm.

3.3. Coulomb failure stress

The Coulomb failure stress change ($\Delta\sigma_{cfs}$) can be estimated to understand earthquake interactions. Also, $\Delta\sigma_{cf}$ assesses the next seismic hazards related to tectonic loading due to past seismicity (Liu *et al.*, 2024). When an earthquake causes permanent deformation of the surrounding medium, the stress field changes on nearby faults (Asayesh *et al.*, 2019). A measure of this change is calculated using $\Delta\sigma_{cfs}$, which can be expressed as,

$$\Delta\sigma_{cfs} = \Delta\tau_s + \mu'\Delta\sigma_{n'}. \tag{3}$$

Here, $\Delta\sigma_{cfs}$ is the change in failure on the receiver fault originating from the strength of the fault (King *et al.*, 1994), $\Delta\tau_s$ is the change in shear stress acting on the receiver fault (positive in the fault slip direction), $\Delta\sigma_n$ is the change in normal stress acting on the receiver fault (positive in extension), and μ' is the effective coefficient of friction on the fault (Toda *et al.*, 2011). The effective coefficient of friction is considered 0.4 in an elastic half-space with uniform isotropic elastic properties (King *et al.*, 1994; Stein *et al.*, 1994). For the source fault geometry, a Poisson ratio of 0.25, a shear modulus of 3.2×10^5 bars, and Young modulus of 8×10^5 bars were used (King *et al.*, 1994; Toda *et al.*, 2011). Generally, changes from 0.1 to 1 bar in $\Delta\sigma_{cfs}$ are considered sufficient to trigger future earthquakes (Yadav *et al.*, 2012; Zarei *et al.*, 2019). The Coulomb stress changes are calculated using the Coulomb 3.4 software package (Toda *et al.*, 2011).

3.3.1. Data for Coulomb stress change

We took the earthquake data for the KTJ and its surroundings with coordinates 38.50°E-41.00°E and 39.00°N-40.00°N. The data for the calculation of the Coulomb stress changes (in bars) were provided by the Global Centroid Moment Tensor (GCMT) and United States Geological Survey (USGS) earthquake catalogues listed in Table 5 (GCMT, 2024; USGS, 2024) and consisted of date, depth, magnitude, longitude, latitude, strike/dip/rake, and source. In the period ranging from 2003 to 2023, we chose 15 local earthquakes with a magnitude greater than $M_w \geq 5.0$. The focal mechanism solutions of selected earthquakes are shown in Fig. 8 with blue beach balls. Since the depth of occurrence for most of the seismicity in the region varied between 0 and 30 km and the earthquakes were predominantly left/right strike-slip faulting mechanisms, we decided on the computational depths of 5, 10, 15, and 20 km for Coulomb stress maps (Fig. 8) with vertical cross-sections down to 30 km of depth (Fig. 9). In the stress change figures, the blue bars (blue lobes) represent the regions with the decreased stress change, and the red bars (red lobes) represent regions with increased stress change.

Going through the main fault and fault zones in the region, except for the complexity of local stress lobes of C-C′, E-E′, and F-F′, vertical cross-sections may be directly divided into positive or negative lobe areas. Especially in sections A-A′, B-B′ and D-D′, positive and negative lobes can be clearly distinguished. In addition to this, based on the distribution of these earthquakes that occurred in previous years, the increased-stress lobes (≥0.0 bar) are predominantly observed in the Kargapazarı segment, Elmalı segment, Bahçeköy Fault,

Table 5 - Focal parameter solutions of earthquakes were collected from the GCMT (2024) and USGS (2024) to calculate Coulomb stress changes in the study region.

No.	Date (dd/mm/yy) (hh:mm:ss)	Depth (km)	Magnitude (M_w)	Longitude (°E)	Latitude (°N)	S/D/R (°)	Source
1	27/01/2003 05:26:30	15.0	6.0	39.660	39.580	152°/75°/-178°	GCMT
2	01/05/2003 00:27:11	15.0	6.3	40.530	39.040	333°/67°/-171°	GCMT
3	28/03/2004 03:51:10	18.9	5.6	40.874	39.847	179°/79°/2°	USGS
4	12/03/2005 07:36:15	16.1	5.6	40.790	39.420	191°/70°/-15°	GCMT
5	14/03/2005 01:56:10	12.0	5.8	40.770	39.440	287°/75°/-165°	GCMT
6	23/03/2005 21:44:56	15.1	5.6	40.710	39.420	188°/77°/-13°	GCMT
7	06/06/2005 07:41:33	15.4	5.6	40.870	39.440	293°/71°/-167°	GCMT
8	10/12/2005 00:09:50	20.3	5.4	40.946	39.394	277°/76°/-177°	USGS
9	02/07/2006 19:39:39	15.0	5.0	40.960	39.274	290°/63°/-163°	USGS
10	25/08/2007 22:05:53	17.4	5.3	40.930	39.370	55°/69°/-10°	GCMT
11	30/07/2009 07:37:51	12.0	5.0	39.726	39.588	137°/49°/-98°	USGS
12	02/12/2015 23:27:09	11.5	5.4	40.255	39.283	208°/79°/27°	USGS
13	14/06/2020 14:24:29	13.5	5.9	40.707	39.423	174°/83°/0°	USGS
14	15/06/2020 06:51:31	11.5	5.5	40.748	39.423	272°/87°/163°	USGS
15	25/06/2021 18:28:37	11.5	5.4	40.167	39.187	319°/39°/-156°	USGS

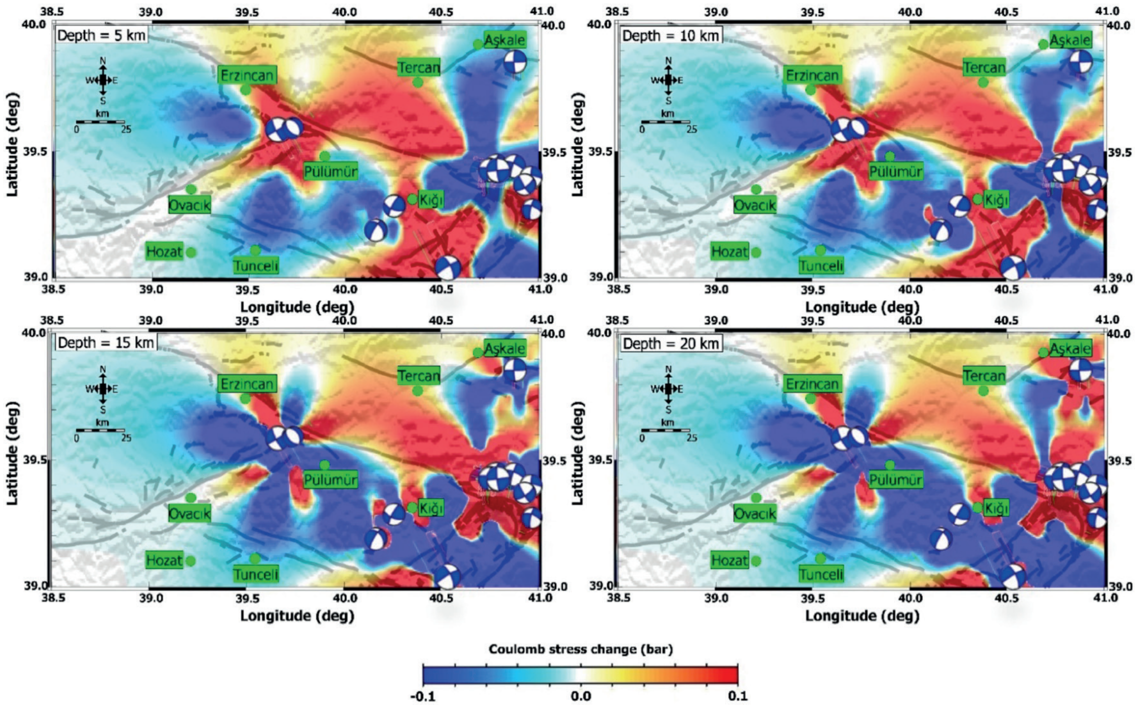

Fig. 8 - Coulomb stress changes (in bars) generated by earthquakes with a magnitude greater than $M_w \geq 5.0$ at depths of 5, 10, 15, and 20 km for the 2003-2023 period (for details see Table 5). Focal mechanism solutions represented by blue beach balls were taken from the GCMT (2024) and USGS (2024) websites. The black lines indicate the active faults in the study region modified by Emre *et al.* (2018). The green circles indicate the city locations. All calculations assumed an effective coefficient of friction (μ) of 0.4 in harmony with the strike-slip fault mechanism.

Karlıova segment, Sancak-Uzunpazar Fault, and Sudüğünü Fault around the KTJ, along the OF, and the region between the Yedisu and Erzincan segments of the NAFZ, and the Tercan Fault on all Coulomb stress maps. This stress accumulation is thought to trigger seismicity in the surrounding areas.

The horizontal displacement vectors of the 2020 earthquakes, which occurred near the KTJ in the study region and had a similar focal mechanism, provided an image compatible with the right lateral strike-slip fault mechanism of the Kargapazarı segment. Considering the reference displacement arrows, a horizontal displacement of 5-6 cm occurred in the NW and SW directions. According to the TADAS (2024), the peak ground acceleration (*PGA*) values of these moderate earthquakes were in the range of 0.06-0.17 g. This region (Bingöl province) has the highest earthquake generation potential. However, the 2015 and 2021 earthquakes that occurred in the area between the Sudüğünü, Sancak-Uzunpazar, and Nazimiye faults (right-lateral strike-slip) located in the west of the Karlıova segment have right-lateral strike-slip and oblique-normal fault mechanisms. We have also calculated the horizontal displacement vectors of five local earthquakes with magnitudes greater than $M \geq 5.0$ that occurred in the study region (Fig. 10). The horizontal displacements are calculated for comparison with GNSS surveys. In addition, Fig. 10 shows the *PGA*, peak ground velocity (*PGV*), and peak ground displacement (*PGD*) values, and the focal mechanism solutions of five earthquakes selected from the AFAD website (https://www.afad.gov.tr/).

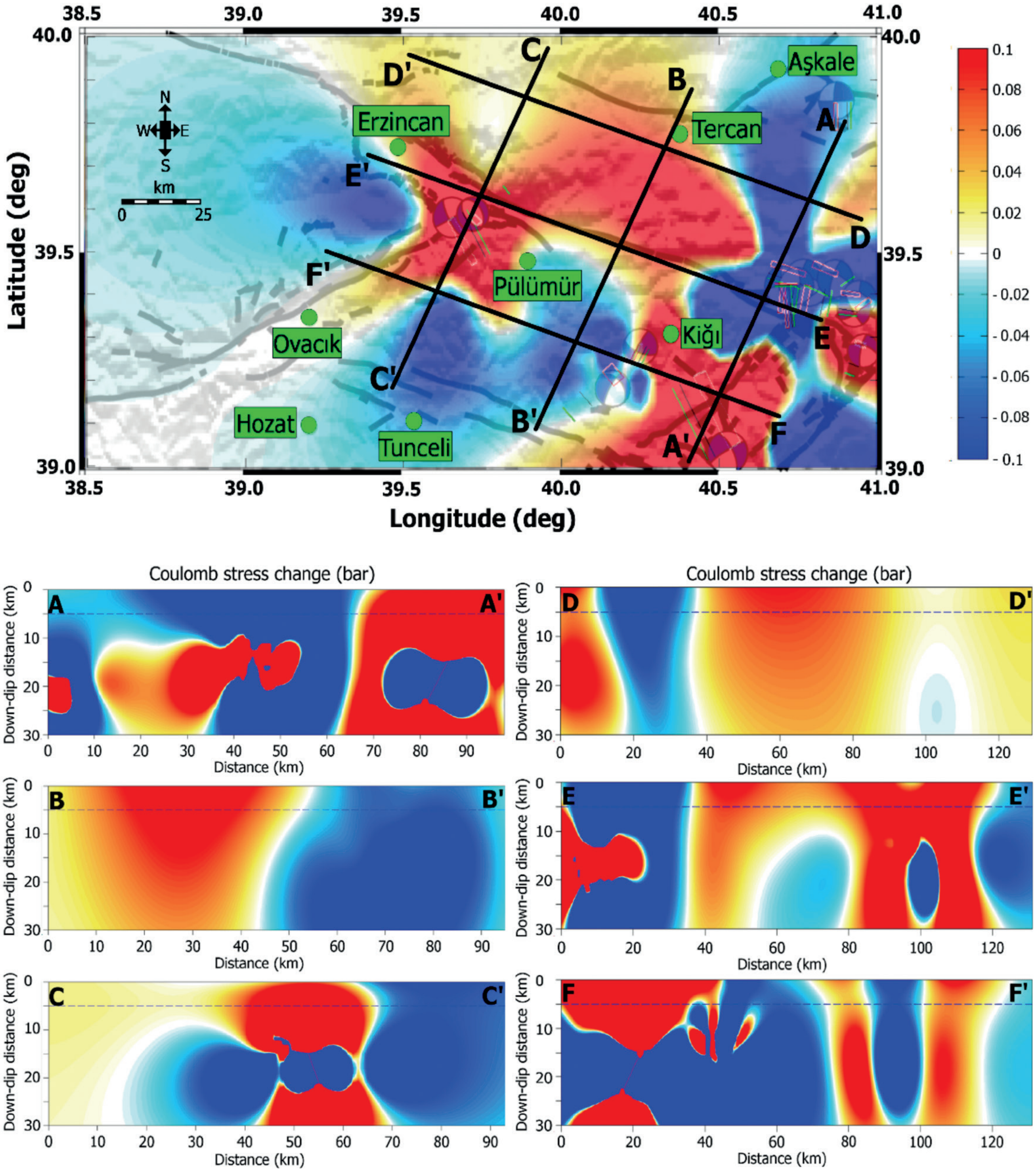

Fig. 9 - NE-SW (A-A’, B-B’, C-C’) and NW-SE (D-D’, E-E’, F-F’) oriented Coulomb stress cross-section profiles from 0 to 30 km, created from focal mechanism solutions shown in Fig. 8. The positive lobes are depicted in red and the negative lobes in blue.

4. Results and discussion

The earthquake activity that started in 2020 on the EAFZ, which had been silent in terms of seismic activity for many years, and progressed towards the south, resulted in two major earthquakes in 2023. According to Alkan *et al.* (2021), the positive stress values transferred in

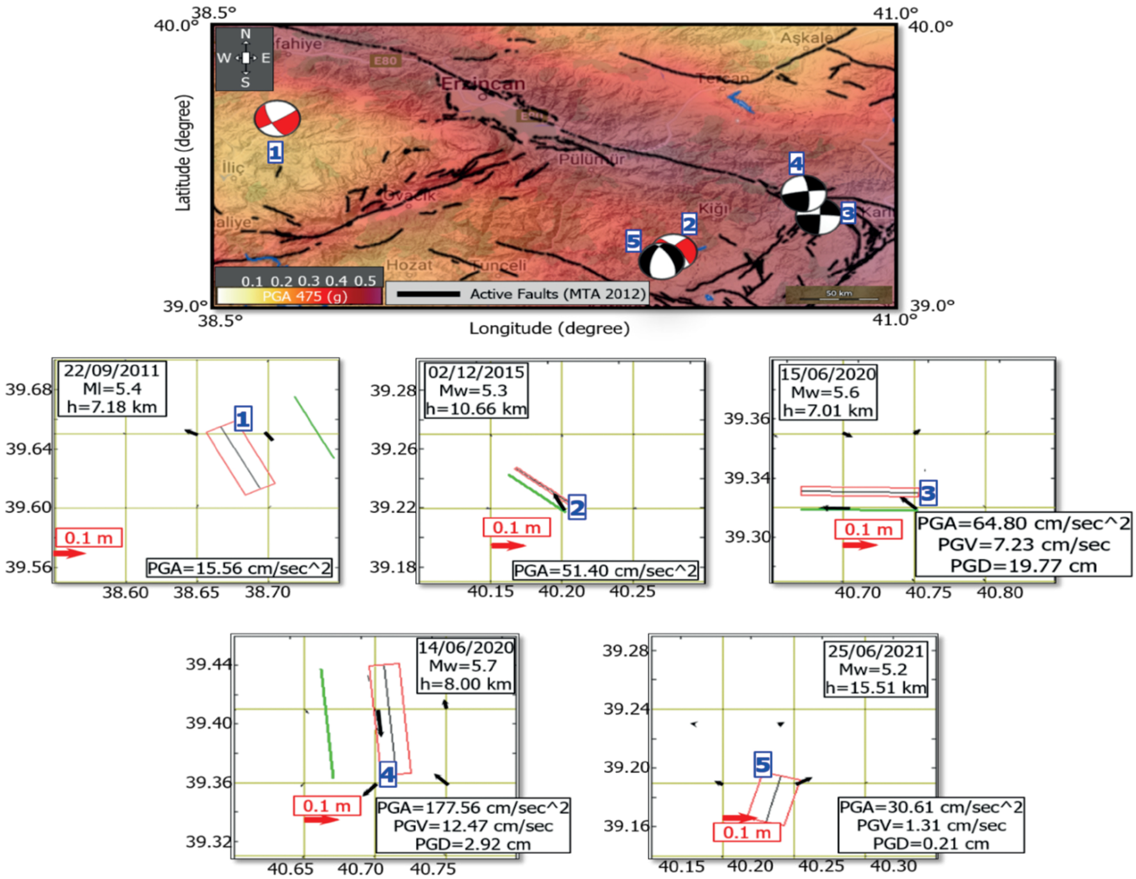

Fig. 10 - Horizontal displacement vector analyses for five local earthquakes with magnitudes greater than $M \geq 5.0$ in the study region. Black lines depict active fault zones taken from Emre *et al.* (2013). Catalogue information, *PGA*, *PGV*, and *PGD* values (the 1st and 2nd earthquakes have no *PGV* and *PGD* information), and focal mechanism solutions of earthquakes are shown in the centre of the figure taken from the AFAD (2024) website. Five small rectangles indicate the horizontal displacement vectors. The black arrows depict the displacement of each earthquake. These figures were obtained from the Coulomb 3.4 software and modified with Zabcı *et al.* (2017).

the Karlıova-Bingöl, Palu-Hazar Lake, and Hazar Lake-Sincik segments at the moderate depth intervals in the north-eastern part of the EAFZ. Besides, in the south-western part of the EAFZ, the stress variations were positive with moderate values in the Çelikhan-Gölbaşı, Gölbaşı-Türkoğlu, and Türkoğlu-Antakya segments, oriented strike-slip fault mechanisms (Alkan *et al.*, 2021). This seismic activity resulted in two major earthquakes in 2023. Therefore, stress tests performed in the present paper (Figs. 8 and 9) have shown that the increasing stress effects around Bingöl-Karlıova in the north create the potential for major earthquakes in this region. This situation was examined in detail within the scope of this study. Karlıova and its surroundings, defined as the triple junction where NAFZ, EAFZ, and NEAFZ intersect, were chosen as the target region. Gravity anomalies around this region were first examined. An attempt was made to establish the relationship between the faults observed on the surface and the gravity anomalies. When the Bouguer gravity anomaly map of Turkey is examined, it is seen that eastern Anatolia consists of negative anomalies due to the crustal thickness being greater than central and western Anatolia. Ates *et al.* (2012) defined the crustal thickness value for this area as 38-40 km. In addition, gravity anomalies vary due to different elevations and geomorphological conditions around the study region. Maden and Öztürk (2015) identified a thick crustal structure regarding large negative gravity anomalies and low *b*-values around the EAFZ and BZSZ. Lower gravity values are observed to be parallel to the basin opening in the form of a band along the south of the NAFZ up to Karlıova (Fig. 3). Higher gravity values are observed in the southern and northern parts of the region. Conversely, there is a low gravity area in the Erzincan pull-apart basin and fault zones. The sediment thickness of the Erzincan basin, located in the western part of the study region, was modelled using gravity anomalies, thus reaching a thickness of 7 km (Aydin *et al.*, 2019). When tilt transformation is applied to the gravity anomaly map given in Fig. 3, the lineaments affecting the gravity anomalies become evident. Faults (most of which are active), observed in the region and distinguished by previous studies, are observed in the tilt-transformed gravity anomaly map (Fig. 5). Discontinuities defined by both surface faulting and gravity anomalies, which often overlap with surface faulting, show that the study region has a very high seismic potential. At the same time, the earthquakes experienced in the past are the most important evidence of this situation. Geodetic monitoring of displacement around the study region after the recent earthquakes constitutes the other important data in this study. Between 2021 and 2024, horizontal and vertical coordinate differences were calculated for nine or ten CORS-TR GNSS points. The resulting values are presented in Tables 1 to 4 and Figs. 6 and 7. In this context, when the horizontal changes between 2021 and 2024 were examined, the horizontal movement of the ADY1 point was 83.4 cm in the east direction.

Since the ADY1 and MLY1 stations are very close to the two earthquake epicentres, horizontal displacements were obtained in the range of 83-84 cm. For other points (except for points ADY1 and MLY1), the largest horizontal movement was computed at the BIN1 station. The horizontal displacement at the CORS-TR BIN1 point, located on the Bingöl-Karlıova segment (approximately 350 km from the site of the two earthquakes), which is the only unbroken section of the EAFZ, was computed in the NE direction and to be around 10.1 cm. The existence of horizontal and vertical geodetic displacements in the KTJ, located north of the region where important fault zones intersect and where large earthquakes have recently occurred, will inevitably cause stress. For this purpose, the stress state in the study region was defined by performing the Coulomb stress change analysis in the KTJ.

The Coulomb stress change maps and cross-sections are presented in Figs. 8 and 9. The results show a good correlation between positive stress changes and shallow crustal earthquakes from 5 to 10 km in the NW-SE and SW-NE directions in the KTJ, while recent seismicity has shown a complex relationship with the stress change lobes. In this region, the Coulomb stress changes are generally positive in the regions accommodating most of the seismic activity. The result of Coulomb stress modelling for 5 and 10 km depths in the KTJ shows four negative stress lobes with N-S and E-W directions, while four positive stress lobes are shown with NW-SE and NE-SW directions. Also, the north and SW parts of the NAFZ lie in the high-stress zone of the Coulomb stress change pattern at all-depth intervals. This means that high-stress regions, especially those included in Erzincan, Ovacık, and Kiğı provinces, are close enough to failure. Alkan *et al.* (2023) remarked that positive stresses have accumulated along the NAFZ segments called the Kargapazarı, Yedisu, and Erzincan segments. In contrast, positive stress lobes appear in the north and negative stress lobes appear in the south of the NAFZ at increasing depths (15-20 km). This identifies the shallow seismicity in the region shown in Table 5. Conversely, the shallow depths of the NE of the EAFZ, including the Karlıova segment and Sancak-Uzun Pazar Fault, are related to positive stress values. These high-stress values appear to be an indication of future seismicity (Alkan *et al.*, 2021). Based on the recent seismic activity around the Bingöl province, Poyraz *et al.*

(2019) calculated the high Coulomb-stress accumulation in the Karakoçan Fault and the Sancak-Uzunpınar Fault at the shallow depths and they associated positive stressed areas with future seismicity. Akbayram *et al.* (2022) studied an earthquake disaster damage prediction of the Genç district located in the Bingöl seismic gap, surrounded by major seismic sources. They defined SW-NE trending active faults, which produced significant earthquakes and caused permanent damage.

Notably, the YSG is a significant region associated with future seismic activity. This region has not produced any strong earthquakes ($M \geq 7+$) since 1784 (Zabcı *et al.*, 2017). Previous studies on Coulomb stress change along the YSG have demonstrated strong positive stress lobes (Nalbant *et al.*, 2002; Ozener *et al.*, 2010; Öztürk and Bayrak, 2012; Sunbul, 2019; Alkan *et al.*, 2023). Öztürk (2017, 2018) studied the earthquake hazard potential of the eastern Anatolian region using several seismotectonic parameters such as Gutenberg-Richter *b*-values, seismic quiescence *Z*-values, annual probability, and recurrence time of earthquakes. There were remarkable decreases in *b*-value and *Z*-values and higher *Dc*-values in the regions covering the Ovacık Fault, Karakoçan Fault, Pülümür Fault, the western part of the BZSZ, the area along the NAFZ, and the southern part of the EAFZ. However, the Coulomb stress change maps have revealed that the negative stress regions (≤0.0 bar) are prominent in the regions between the south of the OF (cross-section C-C'), the west of the EAFZ (cross-sections F-F' and B-B'), and the east of the Tercan Fault (cross-section A-A') from the surface down to 30 km depth. There is also a negative stress change between the west of the OF and the south of the Erzincan segment, at a depth of 20 km.

The *PGA* and horizontal displacement values along with the KTJ and the main fault zones vary between 0.3-0.5 g and 0.21-19.77 cm, respectively for earthquakes with a return period of 475 years (10% probability of exceedance in 50 years) according to the Turkish Earthquake Hazard Map (AFAD, 2024). The largest horizontal movement from the GNSS survey was observed at the BIN1 station, with a displacement of approximately 10.1 cm in the NE direction. Clearly, the highest parameter values were obtained in this region (Fig. 10). Fault mechanism solutions of these earthquakes indicate normal/strike-slip fault mechanisms.

While the horizontal displacement vector of the 2015 earthquake is approximately 7-8 cm in the NW direction, that of the 2021 earthquake is approximately 3-4 cm in the NE direction. The *PGA* values of these earthquakes ranged between 0.03 and 0.05 g. The 2011 earthquake occurred to the south of the Erzincan segment (right-lateral strike-slip) and north of the OF (left-lateral strike-slip). The solution for the focal mechanism lines up with the right-lateral strike-slip and the NW horizontal displacement vector. This vector, about 3 cm long, lines up with the Erzincan segment. The *PGA* value of this earthquake was 0.015 g.

We selected the epicentres of the five earthquakes closest to the GNSS stations and calculated their horizontal displacement vectors. Notably, there are very few earthquakes with magnitudes greater than 5.0 for which focal mechanism solutions have been developed. As a result, focal mechanism solutions for existing earthquakes were obtained from the AFAD and evaluated. However, CORS-TR GNSS stations are marked on the field, taking into account the locations of faults. Consequently, the 2020 and 2021 earthquakes were correlated with BIN1 stations, the 2011 earthquakes with ERZ2 and RHIY stations, and the 2015 and 2021 earthquakes with TNC1 stations (Figs. 6 and 10).

The BIN1 station, situated just south of the Karlıova segment, Sancak-Uzunpazar Fault, and Sudüğünü Fault, is closely associated with the 2020 earthquakes around the Kargapazarı and Elmalı segments, as well as the 2015 and 2021 earthquakes between the Sancak-Uzunpazar and Nazimiye faults, due to its proximity to these locations. According to the findings, the BIN1 station's four-year horizontal displacement vectors predominantly in the NE-E directions.

The overall movement is towards the NE, consistent with the left-lateral strike-slip motion of the Karlıova segment. The 2020 earthquakes are moving W-NW and S-SW, in line with the compression tectonics of the KTJ and the right-lateral strike-slip motion of the Kargapazarı segment. Conversely, the 2021 earthquake and BIN1 station results are quite compatible with each other. Strain variation maps in this region also indicate the presence of two different positive lobes, SW and NE.

The four-year horizontal displacement vectors, obtained from the ERZ2 station located on the Erzincan segment and the RHIY station located just NW of it, completed a clockwise rotation and produced very similar displacement vectors. When the 2011 earthquake's horizontal displacement vectors closest to these stations are examined, they mostly point NW, which fits with the right-lateral strike-slip mechanism of the Erzincan segment. In this case, the clockwise rotation of the GNSS stations and the horizontal displacement vector of the 2011 earthquake become parallel to each other in the NW direction. Additionally, stress maps in the region along the OF and Erzincan segment reveal positive lobes, especially at shallow depths (5-10 km). The 2011 earthquake hypocentre depth also supports the calculated positive stresses.

Station TNC1, south of the Nazimiye Fault (right-lateral strike slip component) and west of the Sudüğünü Fault (right- or left-lateral strike slip component), showed more complicated motion over the four-year period. The displacement vectors first moved in the NE direction, then in the SW direction, and finally in the W-SW direction. As a result, the total horizontal displacement component vector is in the SW direction. The 2015 and 2021 earthquakes also had horizontal displacement vectors in the NE and NW directions, respectively, and had different focal mechanism solutions. This complex situation demonstrates that this region is influenced by a variety of tectonic structures. Stress change maps calculated for different depths also show negative stress changes for the TNC1 station and its vicinity. However, positive stress values are observed in the region of the segments of the EAFZ located to the east of this region.

5. Conclusions

The Coulomb stress analysis conducted within the scope of this study shows the existence of high-stress concentration in the region between the Erzincan-Pülümür and Tercan-Kiğı provinces. In particular, the positive stress extending to a depth of 10 km between Erzincan and Pülümür, and up to 15 km between Tercan and Kiğı, aligns with the focal depths of earthquakes occurring in this region. When the recent aftershock activity is analysed, the presence of earthquakes with magnitudes of 5.0 and above, mostly in the SW and NW of the study region, can be considered as evidence that the stress moves along these directions. In addition, the positions of the main fault systems on the surface were determined by the tilt transformation performed on the gravity anomalies. The dominant directions and positive anomalies corresponding to structural lineaments are mostly in the NW and SW directions. These positive anomalies are consistent with active structural elements such as the NAFZ and EAFZ, the direction and position of positive stress variations.

GNSS data reveals that strain velocity is mostly present in EW and SE-NW directions. The largest horizontal movement, apart from being observed at the ADY1 and MLY1 stations, was observed at the BIN1 station, with a displacement of approximately 10.1 cm in the NE direction. This occurred in the Bingöl-Karlıova segment, the only uninterrupted section of the EAFZ, located about 350 km from the epicentres of the 2023 earthquake. The presence of horizontal and vertical geodetic displacements in the KTJ, situated just north of the recent major earthquakes and at the intersection of significant fault zones, will inevitably lead to the development of stresses. To address this, the stress situation in the study area was assessed using the Coulomb stress change analysis.

In conclusion, the major fault systems with high seismic potential could trigger a destructive earthquake in the KTJ region and its surroundings, supported by the strong correlation between the results of gravity anomaly analysis, Coulomb stress changes, and GNSS data.

Acknowledgments. The authors are grateful to Giuliana Rossi and the anonymous reviewer for their thorough and meticulous review of this paper. They also thank Lavinia Tunini, Associate Editor, for the editorial handling of our paper. Earthquake catalogue information was sourced from GCMT, USGS, and KOERI. The authors also thank MTA-Turkey for providing gravity data.

REFERENCES

AFAD, 2024: *Turkish Disaster and Emergency Management Presidency.* <https://en.afad.gov.tr> (accessed 5 May 2024).

Akar F., Işık E., Avcil F., Büyüksaraç A., Arkan E. and İzol R.; 2024: *Geotechnical and structural damages caused by the 2023 Kahramanmaraş Earthquakes in Gölbaşı (Adıyaman)*. Appl. Sci., 14, 2165, doi: 10.3390/APP14052165.

Akbayram K., Bayrak E., Pamuk E., Özer Ç., Kıranşan K. and Varolgüneş S.; 2022: *Dynamic sub-surface characteristic and the active faults of the Genç District locating over the Bingöl seismic gap of the east Anatolian Fault Zone, eastern Turkey*. Nat. Hazards, 114, 825-847, doi: 10.1007/S11069-022-05414-8/FIGURES/5.

Akpinar Z., Gürsoy H., Tatar O., Büyüksaraç A., Koçbulut F. and Piper J.D.A.; 2016: *Geophysical analysis of fault geometry and volcanic activity in the Erzincan basin, central Turkey: complex evolution of a mature pull-apart basin*. J. Asian Earth Sci., 116, 97-114, doi: 10.1016/J.JSEAES.2015.11.005.

Aktug B., Dikmen U., Dogru A. and Ozener H.; 2013: *Seismicity and strain accumulation around Karliova Triple Junction (Turkey)*. J. Geodyn., 67, 21-29, doi: 10.1016/j.jog.2012.04.008.

Alkan H., Büyüksaraç A., Bektaş Ö. and Işık E.; 2021: *Coulomb stress change before and after 24.01.2020 Sivrice (Elazığ) Earthquake (Mw = 6.8) on the east Anatolian Fault Zone*. Arabian J. Geosci., 14, 3, doi: 10.1007/s12517-021-09080-1.

Alkan H., Öztürk S. and Akkaya İ.; 2023: *Seismic Hazard implications in and around the Yedisu Seismic Gap (eastern Türkiye) based on Coulomb Stress changes, b-values, and S-wave velocity*. Pure Appl. Geophys., 180, 3227-3248, doi: 10.1007/S00024-023-03342-7/FIGURES/9.

Alkan H., Büyüksaraç A. and Bektaş Ö.; 2024: *Investigation of earthquake sequence and stress transfer in the eastern Anatolia Fault Zone by Coulomb stress analysis*. Turk. J. Earth Sci., 33, 56-68, doi: 10.55730/1300-0985.1898.

Ambraseys N.N. and Jackson J.A.; 2000: *Seismicity of the Sea of Marmara (Turkey) since 1500*. Geophys. J. Int., 141, F1-F6, doi: 10.1046/j.1365-246X.2000.00137.x.

Asayesh B.M., Hamzeloo H. and Zafarani H.; 2019: *Coulomb stress changes due to main earthquakes in southeast Iran during 1981 to 2011*. J. Seismol., 23, 135-150, doi: 10.1007/S10950-018-9797-Y/FIGURES/8.

Ates A., Kearey P. and Tufan S.; 1999: *New gravity and magnetic maps of Turkey*, Geophys. J. Int., 136, 499-502.

Ates A., Bilim F., Büyüksaraç A., Aydemir A., Bektaş Ö. and Aslan Y.; 2012: *Crustal structure of Turkey from aeromagnetic, gravity and deep seismic reflection data*. Surv. Geophys., 33, 869-885, doi: 10.1007/S10712-012-9195-X/FIGURES/11.

Aydin Ö.L., Bektaş Ö., Büyüksaraç A. and Yilmaz H.; 2019: *3D Modeling and tectonic interpretation of the Erzincan basin (Turkey) using potential field data*. Earth Sci. Res. J., 23, 57-66, doi: 10.15446/esrj.v23n1.71090.

Barbot S., Luo H., Wang T., Hamiel Y., Piatibratova O., Javed M.T., Braitenberg C. and Gurbuz G.; 2023: *Slip distribution of the February 6, 2023 Mw 7.8 and Mw 7.6, Kahramanmaraş, Turkey earthquake sequence in the east Anatolian Fault Zone*. Seismica, 2, doi: 10.26443/SEISMICA.V2I3.502.

Büyüksaraç A., Gündoğdu E., Bektaş Ö. and Işık E.; 2024: *Failure mechanism by wrench faulting in central Anatolia*. Eng. Fail. Anal., 156, 107786, doi: 10.1016/J.ENGFAILANAL.2023.107786.

Caroir F., Chanier F., Gaullier V., Sakellariou D., Bailleul J., Maillard A., Paquet F., Watremez L., Averbuch O., Graveleau F. and Ferrière J.; 2024*: Late Quaternary deformation in the western extension of the north Anatolian Fault (north Evia, Greece): insights from very high-resolution seismic data (WATER surveys)*. Tectonophys., 870, 230138, doi: 10.1016/J.TECTO.2023.230138.

Cordell L. and Grauch V.I.S.; 1985: *Mapping basement magnetization zones from aeromagnetic data in the san Juan basin, New Mexico*. In: Hinze W.J. (ed), The utility of regional gravity and magnetic anomaly maps, Society of Exploration Geophysicists, Houston, TX, USA, pp. 246-247, doi: 10.1190/1.0931830346.ch16.

Di Giuseppe P., Agostini S., Lustrino M., Karaoğlu Ö., Savaşçın M.Y., Manetti P. and Ersoy Y.; 2017: *Transition from compression to strike-slip tectonics revealed by Miocene-Pleistocene volcanism west of the Karlıova triple junction (east Anatolia)*. J. Petrol., 58, 2055-2087, doi: 10.1093/petrology/egx082.

Duman T. and Emre Ö.; 2013: *The east Anatolian Fault: geometry, segmentation and jog characteristics*. Geol. Soc., Spec. Publ., 372, 495-529, doi: 10.1144/SP372.14.

Emre Ö., Duman T.Y., Özalp S., Elmacı H., Olgun Ş. and Şaroğlu F.; 2013: *Açıklamalı Türkiye Diri Fay Haritası. Ölçek 1:1.250.000*. Maden Tetkik ve Arama Genel Müdürlüğü, Özel Yayın Serisi-30, Ankara-Türkiye. ISBN: 978-605-5310-56-1

Emre Ö., Duman T.Y., Olgun Ş. and Elmacı H.; 2018: *Active fault database of Turkey*. Bull. Earthquake Eng., 16, 3229-3275, doi: 10.1007/s10518-016-0041-2.

Erdik M., Kamer Y., Demircioğlu M. and Şeşetyan K.; 2012: *23 October 2011 Van (Turkey) earthquake*. Nat. Hazards, 64, 651-665, doi: 10.1007/S11069-012-0263-9/FIGURES/13.

GCMT; 2024: *The Global Centroid-Moment-Tensor*. www.globalcmt.org (accessed May 5).

Günaydin O., Inceyol Y., Cetin H. and Ulukavak M.; 2023: *Fault displacement analysis using a multidisciplinary approach on the Gerede Segment of the North Anatolian Fault Zone*. Soil. Dyn. Earthq. Eng., 164, 107519, doi: 10.1016/j.soildyn.2022.107519.

Gürsoy H., Tatar O., Akpinar Z., Polat A., Mesci L. and Tunçer D.; 2013: *New observations on the 1939 Erzincan Earthquake surface rupture on the Kelkit Valley Segment of the north Anatolian Fault Zone, Turkey*. J. Geodyn., 65, 259-271, doi: 10.1016/J.JOG.2012.06.002.

Işık E.; 2022: *Comparative investigation of seismic and structural parameters of earthquakes (M≥6) after 1900 in Turkey*. Arabian J. Geosci., 15, 1-21, doi: 10.1007/S12517-022-10255-7.

Işık E., Ekinci Y.L., Sayil N., Büyüksaraç A. and Aydin M.C.; 2021: *Time-dependent model for earthquake occurrence and effects of design spectra onstructural performance: a case study from the north Anatolian Fault Zone, Turkey*. Turk. J. Earth Sci., 30, 215-234, doi: 10.3906/yer-2004-20.

Işık E., Avcil F., Arkan E., Büyüksaraç A., İzol R. and Topalan M.; 2023*: Structural damage evaluation of mosques and minarets in Adıyaman due to the 06 February 2023 Kahramanmaraş earthquakes*. Eng. Fail. Anal., 151, 107345, doi: 10.1016/J.ENGFAILANAL.2023.107345.

Karaoğlu Ö., Browning J., Bazargan M. and Gudmundsson A.; 2016: *Numerical modelling of triple-junction tectonics at Karlıova, eastern Turkey, with implications for regional magma transport*. Earth Planet. Sci. Lett., 452, 157-170, doi: 10.1016/j.epsl.2016.07.037.

King G.C.P., Stein R.S. and Lin J.; 1994: *Static stress changes and the triggering of earthquakes*. Bull. Seismol. Soc. Am., 84, 935-953, doi: 10.1785/BSSA0840030935.

Kıranşan K., Akbayram K. and Avci V.; 2021: *Bingöl havzası ve cevresinde aktif tektonizmanın jeomorfoloji üzerine etkileri*. Gümüşhane Univ. J. Soc. Sci. Inst., 12, 1110-1129, doi: 10.36362/GUMUS.941564.

Liu J., Qiu X., Yang J., Liang C., Dai J. and Bian Y.; 2024*: Failure transition of shear-to-dilation band of rock salt under triaxial stresses*. J. Rock Mechan. Geotech. Eng., 16, 56-64, doi: 10.1016/J.JRMGE.2023.03.015.

Maden N. and Öztürk S.; 2015: *Seismic b-values, Bouguer gravity and heat flow data beneath eastern Anatolia, Turkey: tectonic implications*. Surv. Geophys., 36, 549-570, doi: 10.1007/s10712-015-9327-1.

McKenzie D.; 1972: *Active tectonics of the Mediterranean region*. Geophys. J. Int., 30, 109-185, doi: 10.1111/J.1365-246X.1972.TB02351.X.

Miller H.G. and Singh V.; 1994: *Potential field tilt-a new concept for location of potential field sources*. J. Appl. Geophys., 32, 213-217, doi: 10.1016/0926-9851(94)90022-1.

Nalbant S.S., McCloskey J., Steacy S. and Barka A.A.; 2002: *Stress accumulation and increased seismic risk in eastern Turkey*. Earth Planet. Sci. Lett., 195, 291-298, doi: 10.1016/S0012-821X(01)00592-1.

Özener H., Arpat E., Ergintav S., Dogru A., Cakmak R., Turgut B. and Dogan U.; 2010: *Kinematics of the eastern part of the north Anatolian Fault Zone*. J. Geodyn., 49, 141-150, doi: 10.1016/J.JOG.2010.01.003.

Öztürk S.; 2017: *Space-time assessing of the earthquake potential in recent years in the eastern Anatolia region of Turkey*. Earth Sci. Res. J., 21, 67-75, doi: 10.15446/esrj.v21n2.50889.

Öztürk S.; 2018: *Earthquake hazard potential in the eastern Anatolian Region of Turkey: seismotectonic b and Dc-values and precursory quiescence Z-value*. Front. Earth Sci., 12, 215-236, doi: 10.1007/s11707-017-0642-3.

Öztürk S.; 2023: *An evaluation of the characteristic aftershock parameters following the January 24, 2020 MW=6.8 Elazığ-Sivrice (Turkey) earthquake*. Baltica J. Geosci., 36, 63-78, doi: 10.5200/baltica.2023.1.6.

Öztürk S. and Bayrak Y.; 2012: *Spatial variations of precursory seismic quiescence observed in recent years in the eastern part of Turkey*. Acta Geophys., 60, 92-118, doi: 10.2478/s11600-011-0035-z.

Öztürk S., Çınar H., Bayrak Y., Karslı H. and Daniel G.; 2008: *Properties of aftershock sequence of the 2003 Bingöl MD=6.4 Turkey earthquake*. Pure Appl. Geophys., 165, 349-371, doi: 10.1007/s00024-008-0300-5.

Pırtı A.; 2022: *Determination of the motion based on GNSS observations between 2000 and 2021 by using the IGS points on the Polar Regions.* Geod. Cartogr., 48(3), 177–184, doi: 10.3846/gac.2022.14848.

Pırtı A.; 2024: *Investigation and prediction of the 2010 Maule, Chile earthquake by using GNSS on 25, 26 and 27 February 2010*. J. South Am. Earth Sci., 133, 104702, doi: 10.1016/J.JSAMES.2023.104702.

Pırtı A., Hoşbaş R.G., and Yücel M.A.; 2023: *Examination of the earthquake (samos island) in izmir (30.10.2020) by using cors-tr GNSS observations and InSAR data*. KSCE J. Civ. Eng., 27(1), 135-144, doi: 10.1007/s12205-022-0392-y.

Poyraz S.A.; 2023: *An investigation of seismic anisotropy in the crust beneath the western part of the north Anatolian Fault Zone*. Tectonophys., 865, 230037, doi: 10.1016/J.TECTO.2023.230037.

Poyraz S.A., Aksarı D., Ergün T., Teoman U.M. and Pınar A.; 2019: *The December 2nd, 2015 Bingöl, Eastern Anatolia-TURKEY, earthquake (Mw= 5.3): A rupture on optimally oriented fault plane*. J. Asian Earth Sci., 173, 88-97, doi:10.1016/j.jseaes.2018.12.019.

Reilinger R. and Mcclusky S.; 2011: *Nubia-Arabia-Eurasia plate motions and the dynamics of Mediterranean and Middle East tectonics*. Geophys. J. Int., 186, 971-979, doi: 10.1111/j.1365-246X.2011.05133.x.

Reilinger R., McClusky S., Vernant P., Lawrence S., Ergintav S., Cakmak R., Ozener H., Kadirov F., Guliev I., Stepanyan R., Nadariya M., Hahubia G., Mahmoud S., Sakr K., Arrajehi A., Paradissis D., Al-Aydrus A., Prilepin M., Guseva T., Evren E., Dmitrotsa A., Gomez F., Al-Ghazzi R. and Karam G.; 2006: *GPS constraints on continental deformation in the Africa-Arabia-Eurasia continental collision zone and implications for the dynamics of plate interactions*. J. Geophys. Res., Solid Earth, 111, 5411, doi: 10.1029/2005JB004051.

Sançar T. and Akyüz H.S.; 2014: *Kuzey anadolu Fay zonu, Ilıpınar segmenti'nin (Karlıova, Bingöl) paleosismolojisi.* Geologic. Bull. Turk., 57, 35-52, doi: 10.25288/TJB.298727.

Sançar T., Zabcı C., Akyüz H.S., Sunal G. and Villa I.M.; 2015: *Distributed transpressive continental deformation: the Varto Fault zone, eastern Turkey,* Tectonophys., 661, 99-111, doi: 10.1016/j.tecto.2015.08.018.

Sarp G.; 2014: *Evolution of neotectonic activity of east Anatolian Fault System (EAFS) in Bingöl pull-apart basin, based on fractal dimension and morphometric indices*. J. Asian Earth Sci., 88, 168-177, doi: 10.1016/J.JSEAES.2014.03.018.

Şengör A.M.C.; 1979: *The north Anatolian transform fault: Its age, offset and tectonic significance*. J. Geol. Soc. London, 136, 269-282, doi: 10.1144/GSJGS.136.3.0269.

Şengör A.M.C.; 1980: *Türkiye neotektoniğinin esasları*. 1-40 pp.

Şengör A.M.C., Tüysüz O., Imren C., Sakinç M., Eyidoğan H., Görür N., Le Pichon X. and Rangin C.; 2005: *The north Anatolian Fault: a new look*. Annual Rev. Earth Planet. Sci., 33, 37-112, doi: 10.1146/ANNUREV.EARTH.32.101802.120415/CITE/REFWORKS.

Seyitoğlu G., Esat K., Tün M., Oruç B., Pekşen E., Aktuğ B., Kaypak B., Koca B., Balkan E., Mutlu S., Pekkan E. and Çetinkaya D.; 2024: *Newly discovered, the Kayapa-Yenişehir cross-basin fault: as revealed by geological and geophysical studies along the southern branch of the north Anatolian Fault Zone, a possible source of the destructive 1855 Bursa earthquakes*. J. Struct. Geol., 179, 105028, doi: 10.1016/J.JSG.2023.105028.

Stein R.S., King G.C.P. and Lin J.; 1994: *Stress Triggering of the 1994 M=6.7 Northridge, California, Earthquake by its predecessors*. Sci., 265, 1432-1435, doi: 10.1126/SCIENCE.265.5177.1432.

Sunbul F.; 2019: *Time-dependent stress increase along the major faults in eastern Turkey*. J. Geodyn., 126, 23-31, doi: 10.1016/J.JOG.2019.03.001.

TADAS, 2024: *Turkish Accelerometric Database and Analysis System.* <tadas.afad.gov.tr/login> (accessed 5 May 2024).

Topcon; 2024: *Topcon magnet tools*, <mytopcon.topconpositioning.com/support/products/magnet-tools> (accessed May 5)

Toda S., Lin J. and Stein R.S.; 2011: *Using the 2011 Mw 9.0 off the Pacific coast of Tohoku Earthquake to test the Coulomb stress triggering hypothesis and to calculate faults brought closer to failure*. Earth Planets Space, 63, 725-730, doi: 10.5047/EPS.2011.05.010/FIGURES/3.

USGS; 2024: U.S. Geological Survey. <www.usgs.gov/> (accessed May 5).

Yadav R.B.S., Gahalaut V.K., Chopra S. and Shan B.; 2012: *Tectonic implications and seismicity triggering during the 2008 Baluchistan, Pakistan earthquake sequence*. J. Asian Earth Sci., 45, 167-178, doi: 10.1016/J.JSEAES.2011.10.003.

Yücel M.A., Pırtı A., Bayburt S., Bektaş Ö. and Büyüksaraç A.; 2024: *Monitoring crustal movements in Istanbul using GNSS and GIS.* Bull. Geoph. Ocean., 65, 309-326, doi: 10.4430/bgo00457.

Zabcı C., Akyüz H.S. and Sançar T.; 2017: *Palaeoseismic history of the eastern part of the north Anatolian Fault (Erzincan, Turkey): implications for the seismicity of the Yedisu seismic gap*. J. Seismol., 21, 1407-1425, doi: 10.1007/S10950-017-9673-1/FIGURES/6.

Zarei S., Khatib M.M., Zare M. and Mousavi S.M.; 2019: *Evaluation of seismicity triggering: insights from the Coulomb static stress changes after the 30 August 1968 Dasht-e-Bayaz Earthquake (Mw7.1), eastern Iran*. Geotectonics, 53, 601-616, doi: 10.1134/S0016852119050078/FIGURES/7.

Corresponding author: Aydın Büyüksaraç
Çanakkale Onsekiz Mart University,
Çanakkale, Turkiye
Phone: +90 5053870502; e-mail: absarac@comu.edu.tr